Characterization of running with compliant curved legs

Jae-Yun Jun, Jonathan E Clark

Characterization of running with compliant curved legs

Jae-Yun Jun[1,2] **and Jonathan E. Clark**[3]

[1] Sorbonne Universités, UPMC Univ Paris 06, UMR 7222, ISIR, F-75005, Paris, France

[2] CNRS, UMR 7222, ISIR, F-75005, Paris, France

[3] Dept. of Mechanical Engineering, Florida State University, Tallahassee, FL, 32310, USA

E-mail: [1,2]jaeyunjk@gmail.com; [3]jeclark@fsu.edu

Abstract. Running with compliant curved legs involves the progression of the center of pressure, the changes of both the leg's stiffness and effective rest length, and the shift of the location of the maximum stress point along the leg. These phenomena are product of the geometric and material properties of these legs, and the rolling motion produced during stance. We examine these aspects with several reduced-order dynamical models to relate the leg's design parameters (such as normalized foot radius, leg's effective stiffness, location of the maximum stress point and leg shape) to running performance (such as robustness and efficiency). By using these models, we show that running with compliant curved legs can be more efficient, robust with fast recovery behavior from perturbations than running with compliant straight legs. Moreover, the running performance can be further improved by tuning these design parameters in the context of running with rolling. The results shown in this work may serve as a potential guidance for future compliant curved leg designs that may further improve the running performance.

1. Introduction

The natural, elegant and seemingly effortless running motions created by humans and animals veil the rich dynamics involved in running. When humans and animals run, their gravitational potential energy fluctuates in phase with the horizontal kinetic energy [1]. During the first half of stance, as the body decelerates, part of the gravitational potential and kinetic energies are stored in their leg muscles, tendons and ligaments, as strain energy. And, during the second half of stance, this energy is returned in part to the gravitational potential and kinetic energies accelerating the body [2]. Furthermore, there seems to be a preferred stride frequency (i.e., resonant frequency) as function of the animals' size, mass and leg stiffness [3].

These aspects of running can be elegantly captured by reduced-order dynamical models. The interest in (and the value of) studying the running dynamics through reduced-order dynamical models does not reside only in the simplicity that makes them attractive but also in the powerful insight that these models give in capturing the running behavior of animals of diverse size, weight, and leg numbers [3, 4]. Furthermore, when the dynamics of running is parameterized using this type of models, the parameters that describe a locomotive system may be tuned to optimize running performance (such as efficiency, speed, and robustness) to both explain the relationship of these parameters to their running performance and, moreover, serve as a guide for reverse-engineering robotic leg designs.

The simplest and the most general model to describe the dynamics of running is the spring-loaded-inverted pendulum (SLIP) model [5, 6, 7, 8], and for this reason it has been accepted as a template [9] (i.e., a minimalistic model) to model animal running [4] and robot running [10]. However, despite its simplicity and the power that this model enjoys, it also abstracts many aspects of human and animal running, which may be key factors for their dynamic richness. First, in the SLIP model, the role of foot design and the foot contact during stance are lost. Unlike the assumed point contact of the SLIP model, during running the foot may roll over the ground as its center of pressure (CoP) progresses from heel to toe (for heel-striking runners) or from mid-foot to toe (for mid-foot-striking runners) in the sagittal plane [11]. Two major past references on this aspect include *Ringrose*'s model of an hopper with a circular foot [12] and *McGeer*'s passive bipedal running model [13]. *Ringrose* showed that running with a curved foot has a direct relationship between the foot radius and the rate of recovery from pitch angle perturbations [12]. But, the increase of the foot radius is upper bounded by the overcorrection of pitch angle errors resulting in unstable running behavior [12]. On the other hand, *McGeer* showed that in running the centrifugal effect in the sagittal plane has a larger role than gravity, and, as a result, the leg spring is stretched in equilibrium (i.e., the leg configuration for which its compression becomes null) [13]. The position of this equilibrium can be controlled by including a curved foot to the leg design and adjusting its foot radius [13]. In this case, the curved foot seems to moderate the centrifugal effect and consequently the overall running motion [13].

Second, the SLIP model assumes the leg to be straight and prismatic, while humans and animals have segmented legs with joints. The geometric configurations of the humans' and animals' legs depend on their scale and the habitat in which they live [14]. The SLIP model does not allow us to see the effect of the reduction of bending moments about the leg joints achieved by large-sized mammalian animals having upright posture [1, 14] nor to study the price that small animals have to pay by crouching their legs (in terms of the reduction of effective mechanical advantage) to gain forward acceleration, which is crucial for their survival [15]. Furthermore, the geometric configuration of a segmented leg seems to influence the demand for energy production, structural stability and velocity transmission from muscle groups to the leg tip [15]. To overcome the shortcomings of the SLIP model along this aspect, dynamical models with leg segmentation have been proposed to show their influence on running performance [16, 17, 18, 19]. Leg segmentation seems to enlarge the stability region by capturing the nonlinearity of the leg's effective stiffness during stance phase, and a similar pattern seems to be observable during human running [18].

Finally, the SLIP model assumes a constant leg stiffness, while humans and animals change their leg stiffness as a function of the payload [3], surface stiffness [20, 21, 22], desired speed [3, 23, 24] or desired stride frequency [25, 26]. When a model embodies the possibility to change the leg's stiffness during stance, then this possibility can allow a legged system to reduce its peaks of reaction forces with the ground, to increase stability [27], to augment safety factor in human-robot interaction [28], and to reduce energy consumption [29]. Recently, *Riese and Seyfarth* showed the benefit of varying the leg stiffness and the leg's rest length for vertical hopping behavior by adding these adaptions to the SLIP model [30]. They showed that softening stiffness and increasing rest length are required for stable hopping [30]. Precisely these phenomena can be obtained in a natural way by running with curved legs. Moreover, both the stiffness decrease and rest length increase during stance can be achieved with no requirement to actively change their values as we will explain in detail along the presentation of this work.

Hence, we observe that the very simplicity that gives power to minimalistic models (such as the SLIP model) to broaden its applicability range also blinds them at the same time to capture aspects (such as those mentioned above) which might significantly influence the dynamics of running, not being able to give further insight for designing robotic legs.

From a mechanical design perspective, most dynamic running robots have utilized very small (effectively point) feet [31, 32, 33, 34, 35]. This may partially be due to a desire for mechanical simplicity or to demonstrate that dynamic stability does not depend on having a large polygon of support as quasi-static walkers do. One notable exception to this is the hexapedal robot *RHex* [36]. Although initially designed with legs having small footpads, a new set of half-circle legs were designed to facilitate stair climbing [37]. These legs allowed the robot to roll up steps and other obstacles, but it was quickly discovered that these legs also gave better performance on level ground

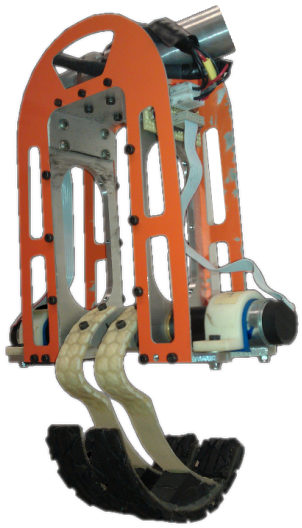

Figure 1. A bipedal robot with curved legs, attached to a boom that constrains the motion of running in sagittal plane.

locomotion as well. Subsequent efforts to tune the '*Buehler-clock*' based controller [36] with these legs have allowed the robot to run at speeds up to 2.7 [m/s] and over very rough terrains [38]. This type of controller uses a periodic function known as the '*Buehler clock*' [36] as the reference trajectory to track the leg motion. This trajectory consists of a periodic two-piecewise linear function with one flatter slope for the slow stance phase and the other steeper slope for the fast swing phase [27].

In the present work, we argue that the good running performance that *RHex* and humans with curved prosthetic legs show is partially because these legs bring together during stance 1) the progression of the center of pressure, 2) variable stiffness, and 3) change of the leg's effective rest length. Interestingly, the advantages that Riese and Seyfarth showed due to the changes of both the variable stiffness and leg's rest length [30] can be achieved passively with curved legs with no direct actuation for generating these changes. This is possible with curved legs mainly because of their geometry and the involved leg circular motion for running.

With the purpose to capture these three changes, a novel reduced-order dynamical model is proposed in the present work. Recently, few works have been published that combine various aspects of *RHex* running that the SLIP model does not capture. Such models include the kinematics of rolling contact and the nonlinear compliance of the leg geometry [39, 40, 41]. Our work differs from these works in the aspects that, by using an articulated leg model with variable location of the maximum stress point along the curved leg, our model is able to capture the progression of the center of pressure, changes in its rest length, the location of its maximum stress point, and the leg stiffness as the leg rolls over the ground. We refer to our novel model as the *Torque-driven and Damped Half Circle Leg* (TD-HCL) model. Finally, we show the benefits of running with curved legs by comparing it first to running with no change at all on the aspects that we aforementioned and then to running with each of the changes. For this purpose,

Table 1. Specifications for the bipedal robot with curved legs shown in Figure 1.

Parameters	**Symbols**	**Values**	**Units**
Body mass	m_{body}	1.026	kg
Body dimension	$W \times L \times H$	$22 \times 24 \times 5.5$	cm $\times$ cm $\times$ cm
Leg mass	m_{leg}	0.045	kg
Leg length (hip to toe)	ζ_o	11.4	cm
Motor stall torque	τ_{s}	0.0569	Nm
Motor no load speed	ω_{nls}	789.6	rad/s
Gear ratio	G_{r}	24 : 1	-

we use in addition to the novel model the SLIP model [7], a two-segment-leg model (with a point foot) [18] and a model that consists of a compliant leg with a rolling foot like the one introduced in [42].

The models that we present in this work are anchored to a bipedal running test robot with curved legs shown in Figure 1 with the purpose to show the experimental results of the present simulation work in the future. The specifications for this robot are shown in Table 1. This robot has been built for testing the performance of running with curved legs in the sagittal plane, and the design parameters have been carefully chosen preserving the dynamic similarity of a *RHex*-like robot known as *EduBot* [43, 44].

The rest of the present work is organized as follows. In Section 2, we propose the model that captures the progression of the center of pressure, leg stiffness change, leg rest length change and the location of the maximum stress point. In Section 3, we study the influence of rolling on running. In Section 4, we show the influence of the leg shape and the location of the maximum stress point on running performance. In Section 5, we compare the running performance obtained from using various reduced-order dynamical models presented in this work. Finally, we summarize our work and suggest areas of future research in Section 6.

2. Torque-driven and damped half-circle-leg (TD-HCL) model

In this section, we propose a model that describes the main aspects of running with curved legs. To the best of our knowledge, *Sayginer* attempted for the first time to characterize running with half-circle legs using a modified version of the SLIP model [39]. We chose to modify the two-segment-leg model instead of modifying the SLIP model because this allows us 1) to characterize the progression of the center of pressure, 2) to represent the variation of the leg stiffness using the Pseudo-Rigid-Body (PRB) model [45], and 3) to describe the change in the leg's effective rest length as well as the change in the location of the maximum stress point. Notice that the PRB model employs a compliant cantilever beam (which resembles the two-segment leg model) and has been often used to characterize the stiffness of actual curved legs [46, 47].

The dynamics of the sagittal-plane running with a half-circle leg can be

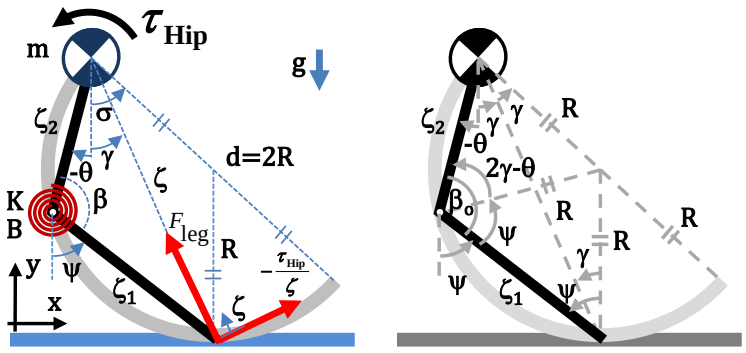

(a) (b)

Figure 2. (a) The torque-driven and damped half-circle leg (TD-HCL) model, a novel model proposed to capture the fundamental aspects of running with a half-circle leg such as the progression of the center of pressure, leg's stiffness change, leg's effective rest length change, and the shift of the maximum stress point along the leg during stance. The parameters and variables that define the model are described in the text. (b) A figure indicating various geometric relationships for a half-circle leg, for the case when the leg is not compressed.

characterized as shown in Figure 2. In this model, the body is represented by a point mass located at the hip with mass m. The massless curved compliant leg is characterized by using two segments with a torsional spring located at the intersegmental joint. The proximal segment (ζ_2) is defined between the hip and the joint of the segments with ζ_{o_2} as its rest length, while the distal segment (ζ_1), between this joint and the contact point of the curved leg with the ground. The latter segment has ζ_{o_1} as its rest length. The leg intersegmental angle (β) is defined as the angle formed by the two segments and has value β_o at rest. The leg's effective length (ζ) is defined as the distance between the position of the center of mass (CoM) and the center of pressure with ζ_o as its rest length. Because the curved leg is assumed to be massless, the two leg segments are also assumed to be massless. The radius of the half-circle leg is represented by R. The position of the center of mass can be represented either using the Cartesian coordinates (x, y) in the inertial frame or the polar coordinates (ζ, γ) attached to the body frame. The energetic losses present in the actual system are modeled using a torsional damper located at the intersegmental joint with a constant damping coefficient (B). To overcome these losses a torque actuator is introduced to the model by attaching it to the hip. In the model, the body is assumed to have an effective infinite inertia. This assumption not only keeps additional complexity from the model (as has been commonly done in analysis of torque-driven SLIP models [48]), but it is also a good estimation of the situation when dealing with multipedal robots that motivated this analysis, where the interaction of the front, middle, and rear legs removes almost all body pitch from the robot [49]. Therefore, the motion of the center of mass is influenced by the gravitational acceleration g and the torque actuation (τ_{Hip}) subject to the interaction of the leg with the ground. All the angles and hip torque are defined to be positive counterclockwisely. A linear

torque-speed curve is used as a simple motor model to delimit the available torque for given angular speed. In the present work, ζ_2/ζ_1=1 is used, where both ζ_1 and ζ_2 vary as function of both the center of pressure and the center of mass.

This model is used to describe the motion of the center of mass of the bipedal running robot shown in Figure 1. A stride consists of two steps (because the considered robotic platform has two legs). However, because we are particularly interested in studying the running behavior (and not walking), we can represent the dynamics of bipedal running representing only one leg in the model by forcing the duty factor to be less than 50% from the controller and by assuming that during flight phase the leg perfectly tracks a given reference trajectory. Therefore, when a leg leaves the stance phase, we track the second leg which is about to make contact with the ground following a given trajectory. Notice that the reference trajectory consists of a periodic two-piecewise linear function with one flatter slope for the slow stance phase and the other steeper slope for the fast swing phase.

Each step consists of two main phases: a stance phase (SP) and a flight phase (FP). Furthermore, the stance phase can terminate either during the leg's rolling motion (stance-rolling phase (SRP)), or during a compliant-vaulting motion over its tiptoe (stance-tiptoe phase (STP)). Therefore, there can be two or three phases within a stride depending on both the leg type and the time instant at which the lift-off event occurs. Three events separate these phases from each other. The transition from stance to flight phase occurs when lift-off (LO) event is triggered, while the transition from flight to stance phase occurs when touch-down (TD) event is detected. Finally, the transition from stance-rolling to stance-tiptoe phase occurs when rolling-to-tiptoe (R2T) event is generated. Therefore a stride can consist of only stance-rolling and flight phases or stance-rolling, stance-tiptoe and flight phases.

The equation of motion for stance-rolling phase (SRP) for running with a curved leg is obtained using the Lagrangian approach as

$$\mathbf{M}(\mathbf{q})\ddot{\mathbf{q}} + \mathbf{N}(\mathbf{q}, \dot{\mathbf{q}}) = \mathbf{Q}, \tag{1}$$

where $\mathbf{M}$, $\mathbf{N}$, and $\mathbf{Q}$ are the inertial matrix, (Coriolis, gravitational and spring) force vector, and external generalized force vector, respectively. The stance-tiptoe phase (STP) is similar to the original two-segment-leg model shown for instance in [18].

The motion of the center of mass during the flight phase (FP) is modeled using a simple ballistic model governed only by gravitational acceleration and is given as

$$\begin{cases} \ddot{x} = 0, \\ \ddot{y} = -g, \\ \ddot{\gamma} = 0, \end{cases} \tag{2}$$

where x, y, γ and g represent the horizontal position of the body, vertical position of the body, leg angle with respect to the vertical line and gravitational acceleration, respectively. During this phase, the leg is assumed to perfectly track a given reference trajectory because the leg is considered to be massless in the model (therefore, there is no moment of inertia) and no air drag force is considered in the model.

The touch-down (TD), lift-off (LO) and rolling-to-tiptoe (R2T) events are triggered by the conditions (3), (4) and (5), respectively.

$$y_{\min} \leq 0, \tag{3}$$

$$F_x \geq \mu F_y, \tag{4}$$

$$\gamma \leq 0, \tag{5}$$

where $y_{\min}$, F_x, F_y, μ, and γ are the distance between the lowest point on the leg and the ground, the horizontal and vertical ground reaction forces, the coefficient of the ground friction and the leg angle with respect to the vertical line, respectively (see Figure 2).

In the following subsections, we describe the details on the modifications added into the two-segment-leg model in order to capture the three main aspects of running with a half-circle-leg.

2.1. Progression of the center of pressure

First, a half-circle leg rolls over the ground producing a progression of the center of pressure until the leg lifts off the ground. When the body angle γ becomes negative while the leg is in contact with the ground, the half-circle leg will not roll anymore but will tip over using its tiptoe. Let us call this leg as *Leg A*. We also considered a circular-shaped leg with an arc length longer than half-circumference. In this case, the leg will continuously roll even with $\gamma<0$. not producing sharp changes in angular velocities due to changes in motion types. Let us call this leg as *Leg B*. In both cases, no slippage due to rolling is allowed in the model. In the present model, two assumptions are made for simplicity: no deformation occurs between the center of pressure and the tiptoe but a circular shape with radius R is maintained during stance; and, for the case of Leg B, the leg can roll as much as it needs until lift-off condition occurs up to a lower limit for the leg angle.‡ The progression of the center of pressure during stance can be expressed as

$$s = 2R(\gamma_{\mathrm{TD}} - \gamma), \tag{6}$$

where s is the arc length, R is the curvature radius, and $(\gamma_{\mathrm{TD}}-\gamma)$ is the difference between the initial angular position (γ_{TD}) corresponding to the time instant at which touch-down event occurs and the instantaneous angular position (γ) after the touch-down event has occurred. The angular position γ is defined positive counterclockwisely. The distance traveled by the center of pressure is equivalent to the arc length traveled until the lift-off condition is triggered (*Leg B*) or until γ becomes zero (*Leg A*).

‡ A lower limit in γ was necessary to be considered in order to avoid the cases in which the leg's effective rest length becomes excessively small.

2.2. Leg stiffness change

The change in the leg's effective stiffness is considered in the present model. This change is caused by the leg's geometry and the displacement of the contact point during stance. *Sayginer* estimated the leg's instantaneous effective stiffness, as the leg rolls, by using the Castigliano's theorem [39]. In the present work, we use the Pseudo-Rigid-Body (PRB) model instead because the difference between the leg stiffness values computed using both methods is relatively small [50], and the leg's instantaneous torsional stiffness value can be easily estimated from the PRB model by using a look-up table published for initially-curved cantilever beams [51]. In addition, the change of the leg stiffness using the PRB model seems to be a natural fit for the TD-HCL model, since the PRB model employs a compliant cantilever beam to characterize the stiffness variation, which resembles the two-segment leg model employed in the TD-HCL model. Further, we fitted the data points shown in this look-up table using polynomial functions to handle cases that this table does not contemplate.

In the PRB model, the torsional stiffness for an initially-curved cantilever beam can be computed as

$$K = \rho K_\Theta \frac{EI}{l}, \tag{7}$$

where K is the torsional stiffness, ρ is the ratio between the length of the pseudo-rigid-body link and the total length of the initially-curved beam, K_Θ is the nondimensional stiffness coefficient, E is the Young's modulus of the material from which the leg is made, I is the second moment of inertia, and l is the total length of the initially-curved beam. In our dynamical model, the torsional stiffness values are computed using E, I and l values published in [44]. A more detailed explanation on how to compute torsional stiffness values using the PRB model can be found in [45].

Intuitively, as the curved leg rolls over the ground the leg becomes softer because the distance between the leg's maximum stress point (represented by the leg's intersegmental joint in the model) and the center of pressure increases. Therefore, the leg's stiffness can be thought as a function of γ as well. We will show later that the results obtained from our model agree with this hypothesis.

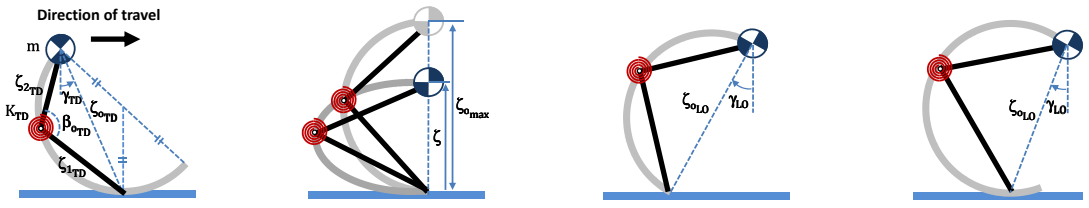

(a) (b) (c) (d)

Figure 3. The leg's effective rest length (ζ_o) becomes longer as the leg rolls over the ground due to how the leg circulates. (a) The effective rest length at touch-down is ζ_o=$\zeta_{o_{TD}}$; (b) The effective rest length when γ=0 is ζ_o=$\zeta_{o_{max}}$; (c) The effective rest length at lift-off for Leg A is ζ_o=$\zeta_{o_{LO}}$; and, (d) The effective rest length at lift-off for Leg B is ζ_o=$\zeta_{o_{LO}}$.

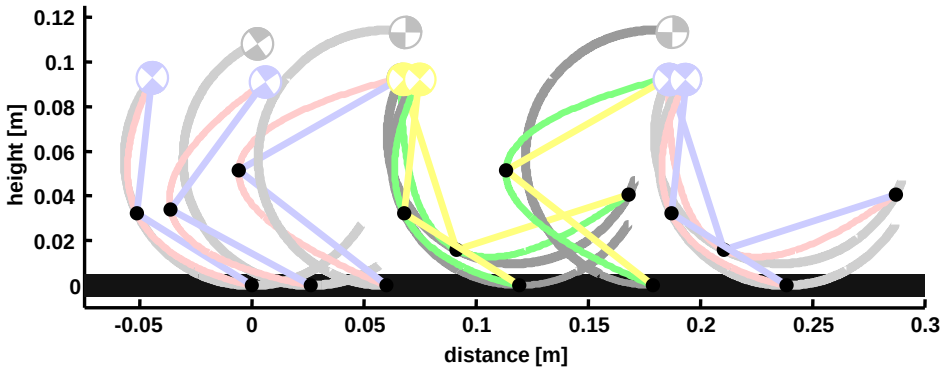

Figure 4. One and a half stride of a steady bipedal running shown by integrating the equations of motion (1) corresponding to the TD-HCL model.

2.3. Changes in the leg rest length and the location of the maximum stress point

As the leg rolls, the leg's effective rest length varies during stance from the time instant at which the leg touches the ground until either it lifts off (Leg B) or it compliantly vaults over its tiptoe (Leg A). Figure 3 shows three representative time instants with their corresponding effective rest length values ($\zeta_{o_{TD}}$, $\zeta_{o_{max}}$, and $\zeta_{o_{LO}}$). These values represent the effective rest lengths at γ=γ_{TD}, γ=0, and γ=γ_{LO}, respectively. For both Leg A and Leg B, the following relationships hold

$$\begin{aligned} \zeta_{o_{TD}} &\leq \zeta_{o_{max}}, \\ \zeta_{o_{LO}} &\leq \zeta_{o_{max}}. \end{aligned} \tag{8}$$

As the leg rolls, the leg's effective rest length (ζ_o), the lengths of the leg segments (ζ_1 and ζ_2), and the intersegmental rest angle obey the following equations

$$\begin{aligned} \zeta_o &= 2R\cos\gamma, \\ \zeta_1 &= \frac{\zeta_o}{\sqrt{1+\chi^2-2\chi\cos\beta_o}}, \\ \zeta_2 &= \chi\zeta_1, \\ \beta_o &= \psi + 2\gamma - \theta, \end{aligned} \tag{9}$$

where χ is the ratio of the lengths of the leg segments, and ψ and θ are the angles formed by the each of the two leg segments with respect to the vertical line (see Figure 2).

2.4. Simulation results obtained using the TD-HCL model

First, Figure 4 shows an example of one stride and a half of a bipedal running gait using the TD-HCL model. The soft and dark colors are used to distinguish the motion of the two legs. The legs with grey color indicate various instantiations of undeflected legs. Blue and yellow colors correspond to the leg segments used in the TD-HCL model. Red and green curves are generated using a cubic spline function built in MATLAB to approximate the deflected leg configurations from the positions of the center of

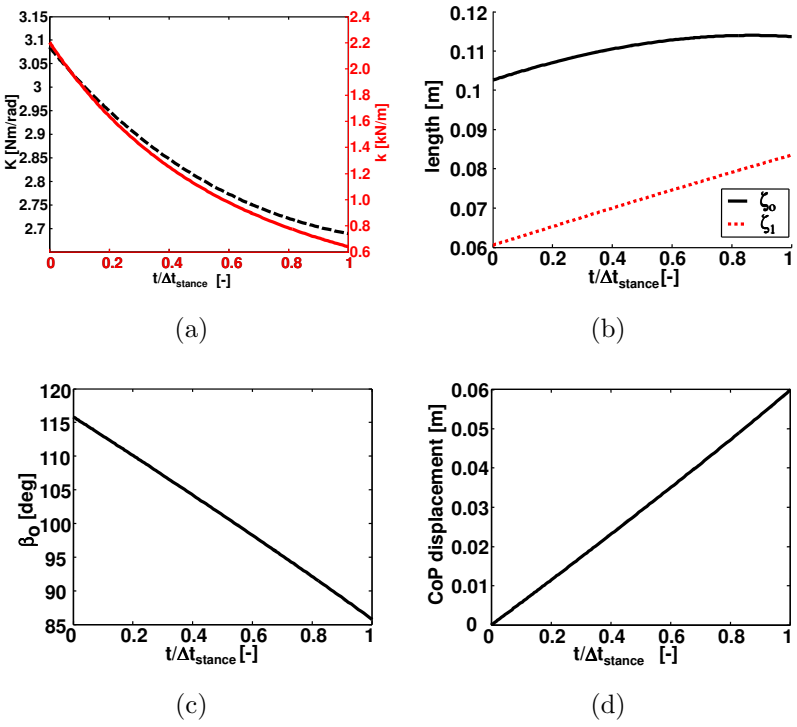

Figure 5. (a) Change in the leg's torsional stiffness values and the equivalent leg's effective axial stiffness values during stance. The relationship between the leg torsional stiffness and the effective axial stiffness is given in [18]; (b) Change in the leg's effective rest length (ζ_o) and the distal segment length (ζ_1) during stance. ζ_2/ζ_1=1 is assumed in the present work, and, therefore, the variation of ζ_2 is not shown; (c) Change in the intersegmental rest angle during stance; and, (d) Progression of center of pressure (CoP) during stance.

mass, knee and center of pressure. Touch-downs of the first leg occur at $x\simeq 0\,[\mathrm{m}]$ and $x\simeq 0.24\,[\mathrm{m}]$, and the touch-down of the second leg, at $x\simeq 0.12\,[\mathrm{m}]$. Lift-off event of the first leg occurs at $x\simeq 0.06\,[\mathrm{m}]$, and the second leg lifts off at $x\simeq 0.18\,[\mathrm{m}]$.

On the other hand, Figure 5 shows the leg torsional stiffness (K), its effective linear stiffness (k), leg rest length (ζ_o), a segment length (ζ_1)§, intersegmental rest angle (β_o) and the displacement of the center of pressure against the stance time for a single step, from the time instant at which the leg touches the ground. Figure 5(a) shows that as the leg rolls during stance its torsional stiffness reduces from about 3.1 [Nm/rad] to about 2.7 [Nm/rad] (which is equivalent to the effective linear stiffness ranging from about 2.2 [kN/m] to about 0.6 [kN/m]). As we have hypothesized, the leg stiffness becomes smaller as the leg rolls over the ground because from the time instant at which the leg touches the ground, the arc length of the leg becomes larger. Here we have shown two different stiffness values: torsional stiffness and the equivalent effective linear stiffness. The torsional stiffness value is obtained from the PRB model as explained previously and shown in (7). The leg's equivalent effective linear stiffness is computed from the

§ The length of one segment is shown only because in this study we assumed that ζ_2/ζ_1=1

torsional stiffness value for the case when the effective leg is compressed 10% of the leg's effective rest length as suggested by [18].

Next, Figure 5(b) shows that the leg's effective rest length increases by about 10 % and the length of the segments increase by about 33 % (shown only the length of the one leg segment because of the condition ζ_2/ζ_1=1 assumed in this study). These increases are due to the fact that the arc length of the leg increases from the touch-down instant until γ becomes zero. The intersegmental rest angle (β_o) also varies during stance as shown in Figure 5(c). This angle decreases from about 115 [deg] to about 85 [deg] for the same reason given previously.

Finally, the displacement of the center of pressure from the time instant of touch-down until when the leg lifts off is shown in Figure 5(d). These results show that the center of pressure displaces about 6 [m] as the leg rolls during stance. This can also be seen in Figure 4. If we focus on the motion of the first leg, we can see that a leg touch-down occurs at x=0 [m] and that the lift-off occurs at $x\simeq$0.06 [m].

In the next two sections, the contribution of each of the two main aspects observed in running with curved legs will be separately studied using a reduced-order dynamical model for each case. These aspects are the progression of the center of pressure (Section 3), and the leg shape and the location of the maximum stress point (Section 4). The individual influence of the variations of the leg stiffness and leg rest length on the running performance are not studied in the present work. A related work (although for hopping) can be consulted from [30].

3. Influence of rolling on running

In this section, we are interested in studying how rolling influences the running behavior. We study this by introducing a reduced-order dynamical model called the *torque-driven and damped spring-loaded-inverted-pendulum with rolling foot* (TD-SLIP-RF). This model is inspired from a model that *Whittington and Thelen* introduced for characterizing the dynamics of human walking for the energy-conservative case [42]. A clock-driven controller is added to the original model for modeling the dynamics of running (instead of characterizing walking).

3.1. Model: torque-driven and damped spring-loaded-inverted-pendulum with rolling foot (TD-SLIP-RF)

The SLIP model is modified by rigidly attaching a non-deformable massless half-circle shaped rolling foot to a compliant leg, and by incorporating a translational viscous damper in parallel to the spring and a torque actuator at the center of mass. A linear torque-speed curve is used as a simple motor model to delimit the available torque for given angular speed. In this model, during stance the leg exerts force against the ground generating reaction force directed from the center of pressure, which is the contact point of the rolling foot with the ground, to the center of mass. As the foot rolls during

stance, the foot's contact point progresses in the horizontal direction. This motion can be described as the expression given in (1), where **M**, **N**, and **Q** now have the following forms:

$$\mathbf{M} = \begin{bmatrix} m & mR\sin(\psi) \\ mR\sin(\psi) & m(\zeta^2 + R^2) + 2mR\zeta\cos(\psi) \end{bmatrix}, \tag{10}$$

$$\mathbf{N} = \begin{bmatrix} -m\zeta\dot{\psi}^2 + b\dot{\zeta} - k(\zeta_o - \zeta) + mg\cos(\psi) \\ 2m(\zeta + R\cos(\psi))\dot{\zeta}\dot{\psi} - mR\zeta\sin(\psi)\dot{\psi}^2 - mg\zeta\sin(\psi) \end{bmatrix}, \tag{11}$$

$$\mathbf{Q} = \begin{bmatrix} 0 \\ \tau_{\text{Hip}} \end{bmatrix}, \tag{12}$$

where m, k, b, R, g, ζ_o, ζ, ψ and τ_{Hip} represent body mass, leg stiffness, leg damping coefficient, foot radius, gravitational acceleration, leg rest length, leg length, leg angle with respect to vertical, and motor torque at the hip, respectively (see Figure 6). Notice that when the radius of the rolling foot becomes zero, (1) becomes the equation of motion corresponding to the torque-driven and damped SLIP (TD-SLIP) model with no rolling [27]. $\mathbf{q}$ and $\dot{\mathbf{q}}$ are generalized coordinates and generalized speeds, respectively, and they have expressions $\mathbf{q}$=$[\zeta, \psi]^T$ and $\dot{\mathbf{q}}$=$[\dot{\zeta}, \dot{\psi}]^T$ (Figure 6). Once again, the flight phase is described using the ballistic model shown in (2).

As shown in [42], the ground reaction force defined from the leg-ground contact point to the center of mass can be expressed in terms of two components (see Figure 6): the force vector along the direction of the leg axis (F_ζ), and the one along the direction of the unit vector of the leg angle (F_ψ). The resulting leg ground reaction force can be expressed as

$$\mathbf{F}_{\text{leg}} = F_\zeta \hat{\mathbf{e}}_\zeta + F_\psi \hat{\mathbf{e}}_\psi, \tag{13}$$

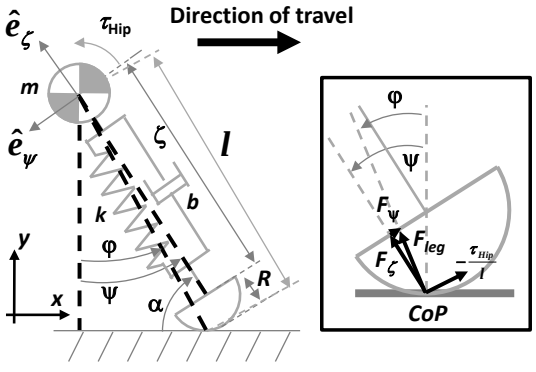

Figure 6. Torque-driven and damped SLIP model with rolling foot (TD-SLIP-RF). The energetic losses are modeled by a translational damper along the leg axis in parallel to the leg spring, where b is the damping coefficient. A torque actuator is added at the hip (τ_{Hip}) to overcome the energetic losses. τ_{Hip} is positive counterclockwisely. See the text for details.

where $\{\hat{\mathbf{e}}_\zeta, \hat{\mathbf{e}}_\psi\}$ are unit vectors along the directions of the leg length and leg angle, respectively, and they are attached to the center of mass. F_ζ and F_ψ can be defined as

$$F_\zeta = k\,(\zeta_o - \zeta) - b\dot{\zeta}, \tag{14}$$

$$F_\psi = -F_\zeta \tan\,(\psi - \varphi), \tag{15}$$

where φ is the angle of the leg-ground reaction force with respect to the vertical line, is positive counterclockwisely, and has the following expression

$$\varphi = \arctan\left(\frac{\zeta \sin\psi}{R + \zeta\cos\psi}\right). \tag{16}$$

The transition from stance to flight (lift-off event) occurs when the vertical ground reaction force becomes less than or equal to zero, or when the following condition is satisfied

$$F_x \geq \mu F_y, \tag{17}$$

where F_x and F_y have the following expressions

$$\begin{array}{rcl} F_x &=& -F_\zeta \sin\psi + F_\psi \cos\psi - \frac{\tau_{\mathrm{Hip}}}{l}\cos\varphi, \\ F_y &=& F_\zeta \cos\psi + F_\psi \sin\psi - \frac{\tau_{\mathrm{Hip}}}{l}\sin\varphi. \end{array} \tag{18}$$

On the other hand, the transition from flight to stance (touch-down event) occurs when the condition to the below is satisfied

$$y \leq \zeta_o \sin\alpha + R, \tag{19}$$

where y is the vertical position of the center of mass, and α is the prescribed leg impact angle with respect to the horizontal line.

3.2. Results

The influence of rolling on running may be studied by relating the foot radius to the running performance (where zero radius represents running without rolling, that is, with a point foot). Two performance measures are considered to show the benefits of rolling: robustness and efficiency. The gait robustness is studied for the energy-conservative system (i.e., neither damper nor actuator are considered), while the efficiency is studied for the actuated system.

3.2.1. Relation between rolling and robustness First, the relation between rolling and gait robustness is established by considering a two-dimensional domain formed by the leg impact angle (α) and the leg stiffness for a variety of foot radius (R) values for the energy-conservative case. We are hereby interested in knowing the range of stable leg impact angles for a given set of leg design parameter values (such as the leg stiffness and foot radius) and a given set of initial conditions $((y_o, v_{x_o})=(L\,[\mathrm{m}], 2.5\,[\mathrm{m/s}]))$ at leg touch-down, where $L=\zeta_o + R$. The larger this range is, the more robust running is, because a legged system can run stably for all the leg impact angles within this stable range. In this study, a gait is considered as stable when the legged system can

run forwardly at least N=50 [strides]. The results are shown in Figure 7. The leg impact angle is shown on the horizontal axis with a precision of 0.1 degree and the leg stiffness, on the vertical axis with a precision of 10 [N/m]. Each surface shown in Figure 7 corresponds to each different normalized foot radius value (R/L) considered. The colored surfaces drawn in each sub-figure represent stable-gait surfaces, while the white regions represent unstable-gait regions. Finally, the color map employed in the sub-figures represents the converged forward speed after N strides (N=50).

From the Figure 7 we see that, as the normalized foot radius is increased, the stability region is enlarged in both directions of leg impact angle and of leg stiffness. When the running is modeled without rolling (i.e., R/L=0, with pin joint contact), the minimum required leg stiffness value for stable running is around 700 [N/m] (Figure 7(a)). Whereas, when the running is modeled with rolling, then the minimum leg

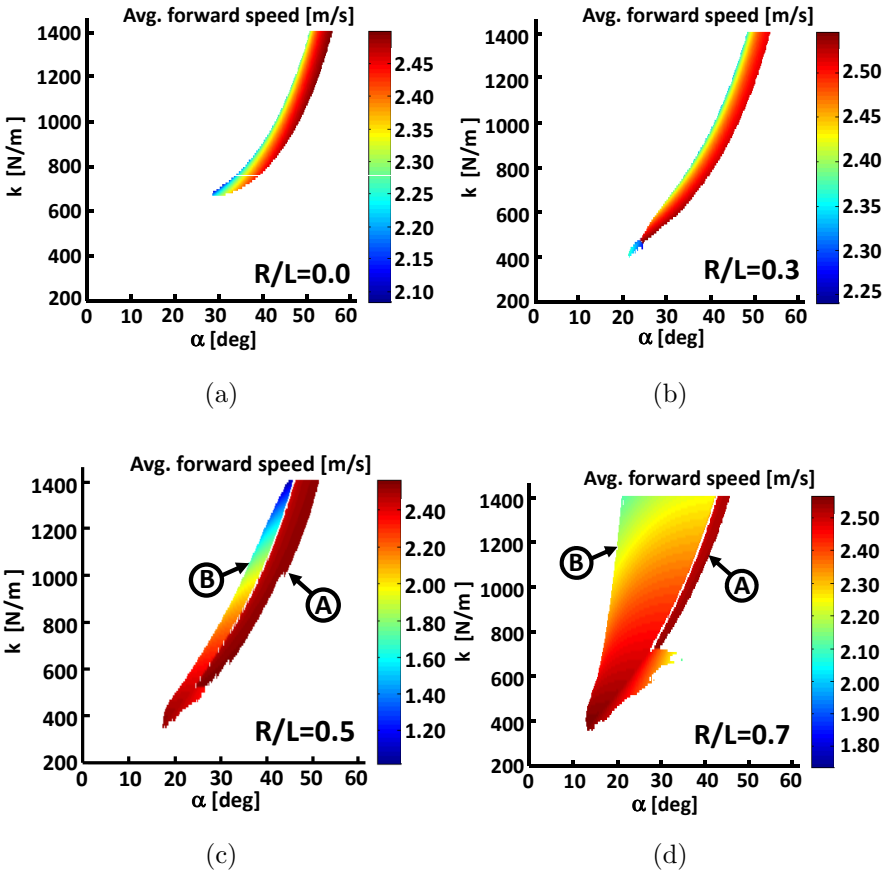

Figure 7. Analysis of gait robustness and running forward speed for various leg stiffness and leg impact angle values. The results shown hereby correspond to the energy-conservative case, and, therefore, in the TD-SLIP-RF model, τ_{Hip}= 0 and b=0 are employed. (a) R/L=0, (b) R/L=0.3, (c) R/L=0.5, and (d) R/L=0.7, where R is the foot radius, and L is the leg total rest length. The meaning of the labels A and B used in (d) are explained in the text. For clarity, the plots corresponding to four R/L values are only shown.

stiffness value for stable running is found around 400 [N/m] (Figures 7(b) – 7(d)).‖ In addition, as the normalized foot radius is increased from 0.0 to 0.7, the maximum range of stable leg impact angles increases from about 7 degrees to about 25 degrees. Furthermore, as the normalized foot radius is increased, the stable-gait surface, while becoming larger, originates two separate surfaces (see Figure 7(c) and Figure 7(d)). These stable-gait surfaces represent two different families of running gaits. The first family corresponds to running gaits with higher running speed, lower apex height and larger leg impact angle (represented as family A in Figure 7(c) and Figure 7(d)). The second family corresponds to running gaits with lower running speed, higher apex height and smaller leg impact angle (represented as family B in Figure 7(c) and Figure 7(d)). The size of the stability surface of the gait family B becomes much larger than that of the gait family A as the normalized foot radius is increased, and the separation of the two regions becomes more obvious. In addition, the speed of the gaits of the family A is almost constant for all stable impact angles and leg stiffness values, while for the gaits of the family B, the running speed is increased as both the leg impact angle and the leg stiffness are decreased.

‖ A similar effect is observed with the leg segmentation. A legged system is able to run at lower leg stiffness as the intersegmental rest angle is increased [18].

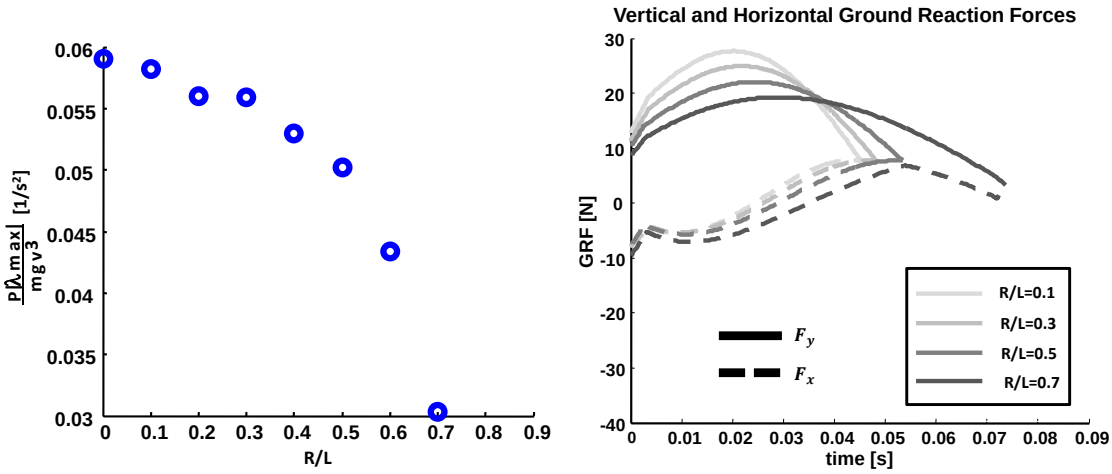

(a) (b)

Figure 8. (a) The values of the specific resistance weighted with the forward speed and the maximum Floquet multiplier (i.e., $P|\lambda_{\max}|/(mgv^3)$) corresponding to various normalized foot radii are shown. The normalized foot radius (R/L) is defined as the ratio of the foot radius (R) to the leg total rest length (L). Each cost value is obtained after optimizing the controller parameters independently. Ten R/L values are considered ranging from 0.0 to 0.9. (b) The vertical and horizontal ground reaction forces are represented against time for various R/L values. For clarity, the plots corresponding to four R/L values are only shown.

3.2.2. Relation between rolling and efficiency For the actuated system, the influence of rolling on running is shown by relating the foot radius to the efficiency. For each value of the normalized foot radius (R/L), the controller parameters are optimized with respect to a speed-weighted version of the specific resistance weighted [52] with the maximum Floquet multiplier [53]) (i.e., $P|\lambda_{\max}|/(mgv^3)$) using the Nelder-Mead algorithm [54]. In this study, we considered ten values of normalized foot radius ranging from R/L=0.0 and R/L=0.9, with the leg stiffness and damping coefficient fixed to be respectively $1,100$ N/m and 32.25 Ns/m (which corresponds to 0.16, as of the damping ratio coefficient). This stiffness value is computed by using the dynamic similarity condition from a small version of the *RHex*-like robot [44], while the damping ratio coefficient has been chosen heuristically. As of the friction coefficient, μ=1.0 is employed. While this is not the only possible objective function or optimization scheme, the resulting gaits seem representative.

Figure 8(a) shows the effect of rolling-related leg design parameter on the running efficiency. First, R/L=0.0 corresponds to the case of pin-joint contact where there is no rolling during stance, and we see that its cost value is higher than for any non-zero value of R/L. This result shows that rolling improves this type of cost function. Furthermore, we see that, as the normalized foot radius (R/L) is increased, the cost value diminishes monotonically reaching its minimum value at R/L=0.7. When R/L is further increased, the foot slips.

In addition, the dynamics of running with differently-sized rolling foot can be studied by looking at their respective ground reaction forces. Figure 8(b) shows the vertical and horizontal ground reaction forces against the stance time. For clarity, the plots corresponding to four R/L values are shown. As the normalized foot radius is increased, the legged system runs with a shallower leg impact angle (because of the foot's geometric constraint), and, when R/L= $\{0.8, 0.9\}$, the horizontal normal force becomes more significant than the vertical ground reaction force causing the foot slippage.

4. Influence of the leg shape and the location of the maximum-stress point on running

In this section, we are interested in studying the influence of the leg shape and the location of the maximum-stress point on running performance such as gait robustness and efficiency. In this study, we do not allow the leg to roll in order to eliminate its influence on the performance (instead we assume a pin joint contact model). We evaluate the influence of leg shape by using a reduced-order dynamical model called the *torque-driven and damped two-segment-leg* (TD-TSL) model. This is a version of the two-segment leg model presented by *Rummel and Seyfarth* [18] modified by adding the clock-driven controller employed by RHex-like robots [27].

4.1. Model

As shown in Figure 9, in the TD-TSL model a legged system is modeled as a point-mass body with mass m, with two massless leg segments that have length ζ_1 (for the distal segment) and ζ_2 (for the proximal segment), the intersegmental angle (β, an angle formed by the two leg segments), and a torsional spring (K) at the joint between the two segments (which models the compliance of the leg). In addition, a torsional damper (B) is considered at the intersegmental joint to model the energy loss, and a torque actuator (τ_{Hip}) to supply the required energy for a steady locomotion.

In this model, both the leg shape and the location of the maximum stress point can be characterized by two leg design parameters: the leg's intersegmental rest angle (β_o) and the ratio of the lengths of the leg segments (ζ_2/ζ_1) with fixed effective rest length, respectively.¶

Two sets of equations of motion govern the dynamics of this system for the two phases that comprise a stride: stance and flight phases. During stance, the system has two degrees of freedom and can be described with two-dimensional generalized coordinates $\mathbf{q}=[\psi,\theta]^T$, and two-dimensional generalized speeds, $\dot{\mathbf{q}}=\left[\dot{\psi},\dot{\theta}\right]^T$. The motion of the body during stance can again be described using the equation given in (1), where $\mathbf{M}$, $\mathbf{N}$, and $\mathbf{Q}$ have the following expressions

$$\mathbf{M}=\begin{bmatrix} m\zeta_1^2 & m\zeta_1\zeta_2\cos(\psi-\theta) \\ m\zeta_1\zeta_2\cos(\psi-\theta) & m\zeta_2^2 \end{bmatrix}, \tag{20}$$

$$\mathbf{N}=\begin{bmatrix} m\zeta_1\zeta_2\sin(\psi-\theta)\dot{\theta}^2+B(\dot{\psi}-\dot{\theta})-mg\zeta_1\sin(\psi)+K(\beta_o-\pi+\psi-\theta) \\ -m\zeta_1\zeta_2\sin(\psi-\theta)\dot{\psi}^2-B(\dot{\psi}-\dot{\theta})-mg\zeta_2\sin(\theta)-K(\beta_o-\pi+\psi-\theta) \end{bmatrix}, \tag{21}$$

¶ The leg's effective rest length is defined as the distance between the center of mass and the tip of the leg at rest.

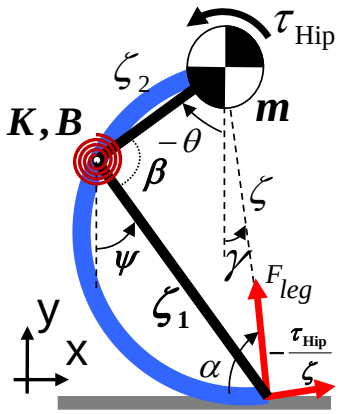

Figure 9. Torque-driven and damped two-segment-leg (TD-TSL) model. A torque actuator (τ_{Hip}) is added at the hip to model the motor that actuates a curved leg, and a torsional damper (B) is incorporated at the intersegmental joint to model the energetic losses of the leg.

$$\mathbf{Q} = \begin{bmatrix} 0 \\ \tau_{\text{Hip}} \end{bmatrix}. \tag{22}$$

The contact force between the leg and the ground defined from the contact point to the robot's center of mass has as magnitude

$$F_{leg} = \frac{\zeta}{\zeta_1 \zeta_2} \frac{K(\beta_o - \beta) - B\dot{\beta}}{\sin \beta}, \tag{23}$$

where $\beta{=}\pi - \psi + \theta$ and $\dot{\beta}{=} - \dot{\psi} + \dot{\theta}$.

The flight phase is described using the ballistic model introduced in (2). The transition from flight to stance (touch-down event) occurs when the condition $y{\leq}\zeta_o \sin\alpha$ is triggered, where α is some predefined leg impact angle with respect to the horizontal line, and y is the height of the center of mass measured from the ground. To trigger the transition from stance to flight (the lift-off event), the Coulomb friction model is employed, as has been done in [48]. That is, the lift-off event occurs when the condition $\mu F_y - F_x{\leq}0$ is triggered, where μ is the coefficient of static friction, and F_x and F_y are the horizontal and vertical ground reaction forces, respectively.

4.2. Results

The influence of the leg shape and the location of the maximum-stress point on running may be studied by relating the intersegmental rest angle and the ratio of the lengths of the leg segments to running performance such as the gait robustness and efficiency. As in the previous section, the gait robustness is studied for the energy-conservative case (i.e., neither damper nor actuator are considered), while efficiency is studied for the actuated system.

4.2.1. Influence of the leg shape and the location of the maximum-stress point on gait robustness

The effect of the leg shape and the location of the maximum stress point along the leg on running is studied by relating the intersegmental rest angle (β_o) and the ratio of the lengths of the leg segments (ζ_2/ζ_1) to the gait robustness for various leg stiffness values for the energy-conservative case. The search for an optimal set of leg design parameters is performed by relating each set of design parameter values to the range of

Table 2. Design parameters and initial conditions

Parameters	**Values**
ζ_2/ζ_1	$\{(0.15 : 0.05 : 1), (1/0.95 : 1/0.05 : 1/0.15)\}$
β_o	$[90^o : 2^o : 170^o]$
$k_{10\%}$	$\{1100, 1900, 2700, 3500\}$ [N/m]
y_o^{apex}	$\{\zeta_o, 1.2\zeta_o\}$ [m]
$v_{x_o}^{\text{apex}}$	$\{1.5, 2, 2.5\}$ [m/s]

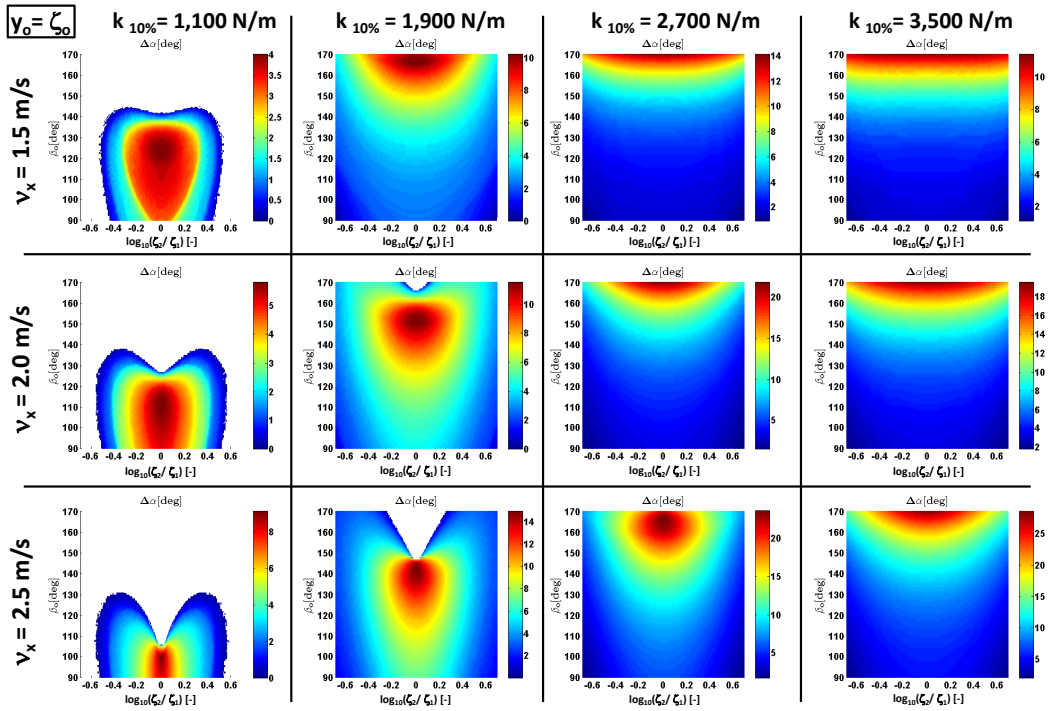

Figure 10. The range of stable leg impact angles ($\Delta\alpha$) is represented for various (ζ_2/ζ_1,β_o) values, for four leg reference stiffness, for three initial forward velocities and for y_o=ζ_o.

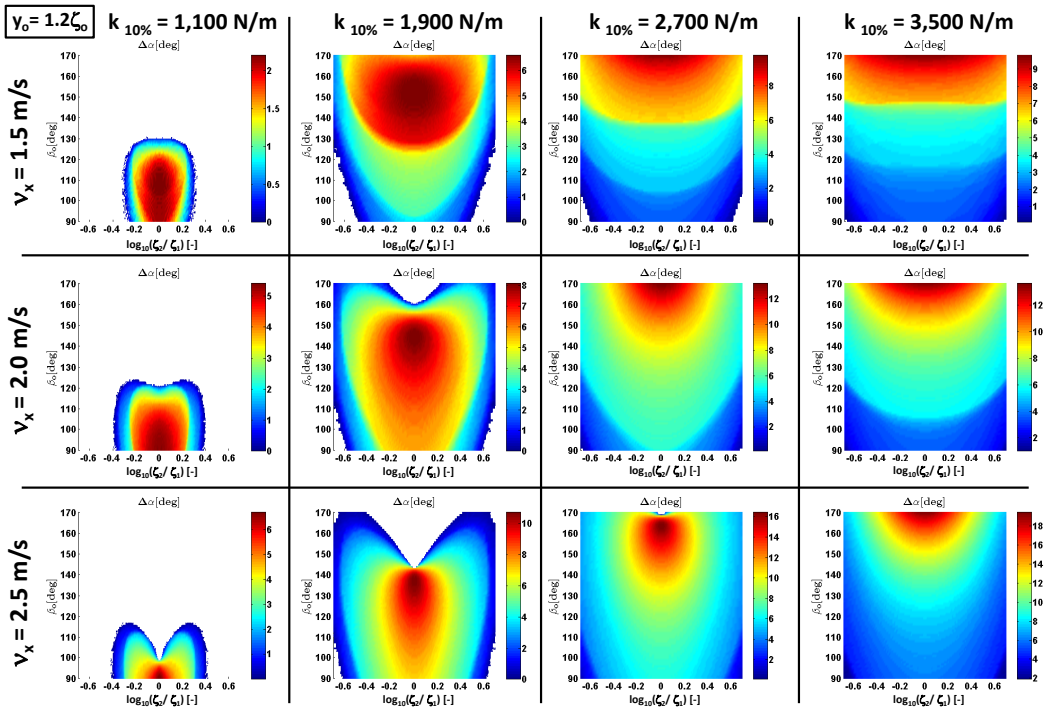

Figure 11. The range of stable leg impact angles($\Delta\alpha$) is represented for various (ζ_2/ζ_1,β_o) values, for four leg reference stiffness, for three initial forward velocities and for y_o=1.2ζ_o.

leg impact angles for which the running gaits are stable. The larger the range of stable leg impact angles is, the more robust running is. A running gait is considered here to be stable by using the strides-to-fall method. That is, a gait is considered stable if the legged system is able to run N strides (N=50) without falling.

As for the leg stiffness, we relate the leg torsional stiffness to the equivalent translational stiffness as *Rummel and Seyfarth* established in [18]. A constant relationship is assumed between the two stiffness values by considering the case when the equivalent translational spring is compressed 10% of the leg's effective rest length. This value has been chosen because the effective leg is compressed about this percentage in average human running [18]. The translational leg stiffness at 10% compression can be computed as $k_{10\%}=F_{10\%}/\Delta\zeta_{10\%}$, where $\Delta\zeta_{10\%}$ is a reference leg compression at 10% of the effective rest length (i.e., $0.1\zeta_o$), and $F_{10\%}$ is the leg force at the reference leg compression.

Hence, our problem reduces to relate the leg design parameters ($k_{10\%}$, ζ_2/ζ_1, β_o) for given initial conditions (y_o^{apex}, $v_{x_o}^{\text{apex}}$) to the range of stable leg impact angles ($\Delta\alpha$). In order to solve this problem, the values shown in Table 2 have been considered.

Figure 10 and Figure 11 show the range of stable leg impact angles ($\Delta\alpha$), represented by a colormap, for the considered design parameters and initial conditions at apex. The 2D-domain on which each surface is depicted is formed by the leg segments' ratios (i.e., the ratio of the length of the proximal segment (ζ_2) to the length of the distal segment (ζ_1)) and the leg intersegmental rest angles (β_o). The horizontal axis (ζ_2/ζ_1) is in logarithmic scale while the vertical axis (β_o) is in linear scale. Note that the white color regions present in some of the plots correspond to the cases of unstable gaits. In these figures, the surfaces of each column correspond to the results obtained for a given leg reference stiffness. Four different leg reference stiffness values have been considered. The surfaces of each row are the results obtained for a given initial forward velocity. The three rows of both Figure 10 and Figure 11 correspond to the considered three initial forward velocities of the center of mass: ($v_{x_o}^{\text{apex}} \in \{1.5, 2, 2.5\}$ [m/s]) with the initial height of the center of mass at $y_o^{\text{apex}}=\zeta_o$ at apex (Figure 10) and at $y_o^{\text{apex}}=1.2\zeta_o$ at apex (Figure 11). For each surface, the considered leg impact angles (α) range from 30^o to 90^o with a precision of 0.1^o.

Both Figure 10 and Figure 11 show that the largest range of stable leg impact angles ($\Delta\alpha$) occurs when $\zeta_2/\zeta_1=1$ for all the considered leg intersegmental rest angles, leg reference stiffness values and initial conditions. The stability region expands in both directions of the 2D-domain formed by the ratio of the lengths of the leg segments (ζ_2/ζ_1) and the leg intersegmental rest angle (β_o) with the leg reference stiffness increase for all the initial conditions considered. For the lowest leg reference stiffness value considered, stable gaits exist only for low leg intersegmental rest angles (see the surfaces of the first column of both Figure 10 and Figure 11).

In general, the range of stable leg impact angles ($\Delta\alpha$) increases with both the leg reference stiffness increase and the initial forward velocity increase. For instance, for $(y_o, v_{x_o})=(\zeta_o, 2\,[\text{m/s}])$, $\Delta\alpha_{\max}$ increases from about 6^o to about 20^o when $k_{10\%}$ is increased

from $1,100$ [N/m] to $3,500$ [N/m]. On the other hand, for y_o=ζ_o and $k_{10\%}$=$1,100$ [N/m], $\Delta\alpha_{\max}$ increases from about 4^o to about 9^o as v_{x_o} is increased from 1.5 [m/s] to 2.5 [m/s].

In addition, the maximum range of stable leg impact angles ($\Delta\alpha_{\max}$, the peak of each surface) shifts from low leg intersegmental rest angle to a larger intersegmental rest angle as the leg reference stiffness value is increased for all the initial conditions considered. For instance, for (y_o, v_{x_o})=$(1.2\zeta_o, 2.5\,[\text{m/s}])$, the location of $\Delta\alpha_{\max}$ shifts from β_o≈90^o to β_o≈170^o as $k_{10\%}$ is increased from $1,100$ [N/m] to $3,500$ [N/m].

Further, the rate of this shift becomes smaller as the initial forward speed of the center of mass increases, for the considered initial height values. Also, running with lower height of the center of mass (the graphs of the first three rows) is in general more stable than running at higher height (the graphs of the last three rows). We observe this phenomenon by realizing that both the size of the stability region and the range of stable leg impact angles are larger for low initial height of the center of mass.

Moreover, the results shown in both Figure 10 and Figure 11 suggest that it is desirable to change the leg's stiffness and intersegmental rest angle in order to run optimally at various forward velocities. This result is in accordance with the results that *Rummel and Seyfarth* showed in [18].

Based on these results, it is desirable to design legs with the same lengths of the proximal and distal segments, that is ζ_2/ζ_1=1. However, ζ_2/ζ_1=1 may require the design of stronger legs because the distance between the maximum stress point and the effective leg axis can be significant as β becomes small, reducing the mechanical advantage [14].

Finally, the two-segment-leg model predicts that for a given leg reference stiffness there exists a leg intersegmental rest angle β_o for which the range of stable leg impact angles ($\Delta\alpha$) is maximized. And, this range ($\Delta\alpha$) increases with the leg intersegmental rest angle when ζ_2/ζ_1=1. Therefore, large leg intersegmental rest angle is desirable for robustness optimality (with the appropriate leg reference stiffness).

4.2.2. Influence of the leg shape and the location of the maximum-stress point on efficiency For the actuated system, we have studied the influence of the leg shape and and the location of the maximum-stress point on running efficiency. Three legs are chosen from Figure 10. As shown in Figure 12, the first leg is the one that represents a half-circle leg with unity-ratio of leg segments (i.e. β_o=90^o and ζ_2/ζ_1=1) (Leg I). The second leg is the one that has the same ratio of leg segments but with an ellipsoidal shape (i.e. β_o=150^o and ζ_2/ζ_1=1) (Leg II). Finally, the third leg is the one that has the shape of a half-circle leg but with a ratio of leg segments different from unity (i.e. β_o=90^o and ζ_2/ζ_1=0.35) (Leg III). As far as the leg stiffness, the value that maximizes the range of stable impact angles is chosen for y_o=ζ_o and v_x=2.5 [m/s]. Therefore, $k_{10\%}$=$1,100$ [N/m], $k_{10\%}$=$2,700$ [N/m], and $k_{10\%}$=$1,100$ [N/m] are chosen for Leg I, Leg II and Leg III, respectively.

For each leg, the parameters of the clock-based controller [27] are optimized for the specific resistance [55], and the results are shown in Table 3. The results indicate that the most efficient gait is obtained by running with Leg I, and the least efficient

(a) (b) (c)

Figure 12. Compliant curved legs with: (a) β_o=90^o, ζ_2/ζ_1=1, $k_{10\%}$=1,100 [N/m] (Leg I); (b) β_o=150^o, ζ_2/ζ_1=1, $k_{10\%}$=2,700 [N/m] (Leg II); (c) β_o=90^o, ζ_2/ζ_1=0.35, $k_{10\%}$=1,100 [N/m] (Leg III).

Table 3. Simulation results by running with the controller parameters optimized for specific resistance

Leg	$\lvert\lambda_{\max}\rvert$	v_x [m/s]	Mechanical Power [W]	SR
I	0.9769	1.1447	5.0909	0.4419
II	0.9419	0.8412	4.3179	0.5100
III	0.8937	1.2757	6.7539	0.5260

one by running with Leg III. Knowing that running with Leg II is more robust than running with Leg I in the energy-conservative case, depending on the leg shape one can achieve a more robust running gait or a more efficient running gait (for the chosen robotic platform shown in Figure 1).

5. Comparison between the considered reduced-order dynamical models for running

In this section, we compare the running performance obtained from various models. These models are shown in Figure 13. In total five different types of legs are considered (Table 4): TD-HCL with tiptoe (Leg A), TD-HCL without tiptoe (Leg B), TD-TSL (Leg C), TD-SLIP-RF (Leg D), and TD-SLIP (Leg E). The TD-SLIP model is described in [27]. For all the models, m=1.026 [kg] and ζ_o=0.114 [m] are used. For TD-SLIP and TD-SLIP-RF, k=1,100 [N/m] is used, while for TD-TSL, torsional stiffness corresponding to this k is computed as in [18].

In addition, for TD-TSL, ζ_2/ζ_1=1 and β_o=90^o are used, and for TD-SLIP-RF, R=0.5L[+] is used (see Figure 13 to identify these parameters). To be able to compare the results obtained from using different models, the controller parameters are independently

[+] $R = 0.5L$ is considered for the TD-SLIP-RF model because the considered leg is a half-circle leg.

Table 4. Definition of legs under study

Leg type	Description
Leg A	TD-HCL model with tiptoe
Leg B	TD-HCL model with no tiptoe
Leg C	TD-TSL model
Leg D	TD-SLIP-RF model
Leg E	TD-SLIP model

optimized using a direct search method, the Nelder-Mead algorithm [54]. In order to avoid local minima in the optimization process, various initial simplexes are used for each leg model. In addition, for a chosen initial simplex, multiple descents have been performed by spreading out the converged simplex points to search for a better convergence. The considered cost functions are the specific resistance (SR) and a speed-weighted version of the specific resistance (SR/v^2). The former objective function measures running efficiency, while the latter one takes into account both running efficiency and forward speed. Details of how the controller parameters are optimized for an objective function using this algorithm are given in [27].

5.1. Results

The comparison results are shown in Figure 14. The horizontal axis for all four plots represents the considered five leg types. Figure 14(a) and Figure 14(c) show the specific resistance and the absolute value of the maximum Floquet multiplier when the controller parameters are optimized for specific resistance. On the other hand, Figure 14(b) and Figure 14(d) represent the specific resistance and the absolute value of the maximum

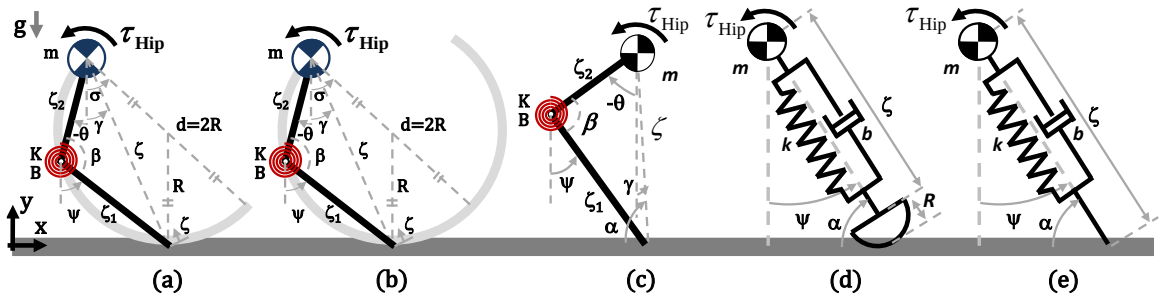

Figure 13. (a) Leg A: Torque-driven and damped half-circle-leg (TD-HCL) model with tiptoe and ζ_2/ζ_1=1; (b) Leg B: Torque-driven and damped half-circle-leg (TD-HCL) model with no tiptoe and ζ_2/ζ_1=1; (c) Leg C: Torque-driven and damped two-segment-leg (TD-TSL) model with ζ_2/ζ_1=1 and β_o=90^o; (d) Leg D: Torque-driven and damped spring-loaded-inverted-pendulum with a rolling foot (TD-SLIP-RF) model with R=$L/2$, where L is the total leg rest length; and, (e) Leg E: Torque-driven and damped SLIP (TD-SLIP) model described in [27].

Floquet multiplier when the controller parameters are optimized for the speed-weighted version of the specific resistance.

Figures 14(a) and 14(b) show that in general running with Leg A, Leg B or Leg D seem to be more efficient (low SR values) than running with Leg C or Leg E (higher SR values). Running with Leg A, Leg B or Leg D involve rolling, while running with Leg C or Leg E, pin-joint contact. These results indicate that more efficient running is possible for legs with rolling contact. Furthermore, we observe from Figure 14(a) that running with Leg D is the most efficient. This is mainly because of low mechanical power requirement compared to running with other legs. In general, the mechanical power consumption with legs that involve rolling (i.e., Leg A, Leg B and Leg D) was lower than running with legs with point foot. Although running with Leg D is more efficient in simulation, this leg is stiff along the orthogonal direction to the leg axis, and, when the leg impacts the ground, the reaction force along this direction can be large (especially with a torque actuator) with possible damage to the leg. On the other hand, running with Leg A or Leg B this impact is less severe since these legs are compliant in

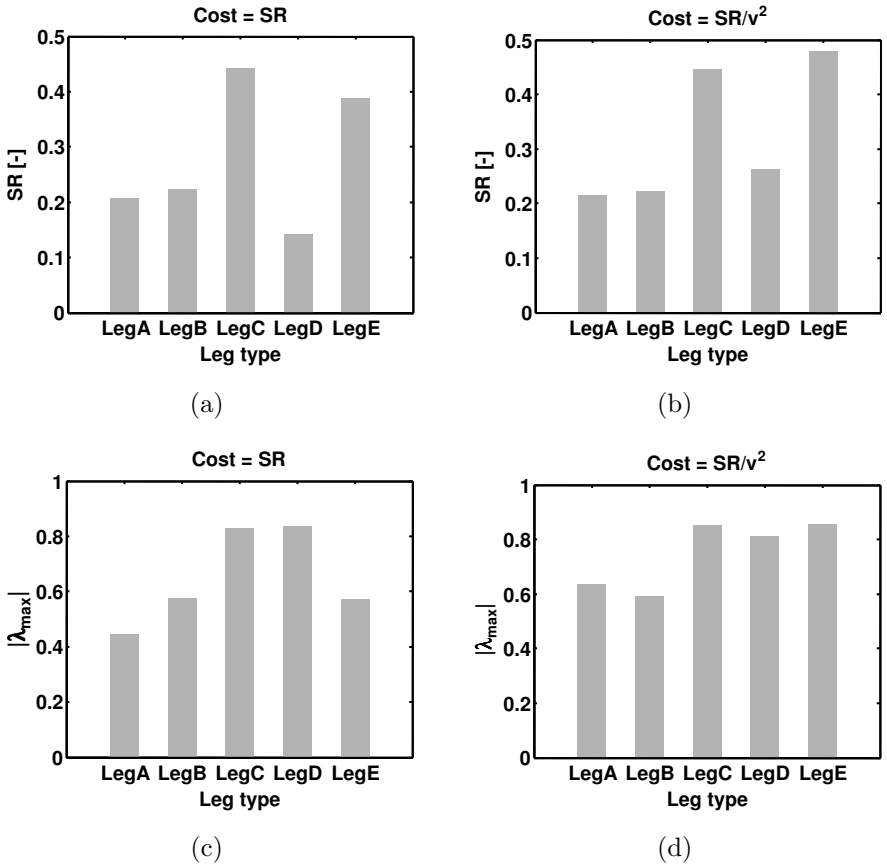

Figure 14. (a) Specific resistance (SR) values for when the considered cost function is precisely SR; (b) Specific resistance (SR) values for when the considered cost function is SR/v^2; (c) Values of 2-norm of the maximum Floquet multiplier for when SR is the cost function; and, (d) Values of 2-norm of the maximum Floquet multiplier for when SR/v^2 is the cost function.

both axial and radial directions in the sagittal-plane.

Figures 14(c) and 14(d) show that in general the maximum Floquet multiplier is the smallest for the cases of running with either Leg A or Leg B. This indicates that when a perturbation is applied to a steady gait, running with compliant curved legs can recover from the perturbation requiring the smallest amount of time than running with other types of legs.

6. Conclusion

A novel reduced-order dynamical model, called the *torque-driven and damped half-circle leg* (TD-HCL) model, is proposed to show the benefits of running with compliant curved legs. This model captures three main aspects of running with such legs: 1) the progression of the center of pressure, 2) variation of the leg stiffness, 3) change in the leg's rest length (and the associated shift of the location of the maximum stress point). The performance of running with a curved compliant leg (represented by the TD-HCL model) is compared to that of running with a straight compliant leg (represented by the TD-SLIP model). The comparison results show that curved compliant legs offer a running gait that is more efficient and that allows the legged system a faster recovery from perturbations than straight compliant legs do.

In addition, some of the characteristics of running with curved compliant legs are individually analyzed with dedicate reduced-order dynamical models. The progression of the center of pressure is captured using the *torque-driven and damped spring-loaded-inverted pendulum with a rolling foot* (TD-SLIP-RF) model and is parameterized with the radius of the rolling foot. As the foot radius increases, the running is more robust and more efficient, and the variation of the vertical ground reaction force becomes smoother. But, the increase of the foot radius is limited by the foot slippage because as the foot radius increases the desired touch-down angle flattens more increasing in this way the horizontal ground reaction force.

Further, the leg shape and the location of the maximum stress point along the leg also affects the performance of running. These aspects are studied using the *torque-driven and damped two-segment leg* (TD-TSL) model. In this model, the leg is characterized with two segments. The leg shape is described with a model parameter known as the intersegmental joint angle (β), and the location of the maximum stress point is represented by the ratio between the lengths of the two segments (ζ_2/ζ_1). For all the considered leg shapes and leg stiffness values, the maximum robustness is always achieved when the maximum stress point is on the middle of the effective leg (i.e., ζ_2/ζ_1=1). On the other hand, the robustness increases as the leg shape becomes more open (i.e., larger β) or the leg stiffness increases. In addition, a running gait is more efficient when the maximum stress point is on the middle of the effective leg and the leg shape is circular.

Moreover, the proposed reduced-order dynamical model (TD-HCL) is not only limited to describe half-circle legs but it can easily represent other curved leg shapes by

simply changing both the intersegmental rest angle and the ratio between the lengths of the two segments. We believe that this model can also be useful for characterizing and improving the design of curved prosthetic limbs which are often used for running or jogging.

As future work, other running performance measures than the largest Floquet multiplier, specific resistance or a speed-weighted version of the specific resistance considered in this work may be interesting such as the gait sensitivity norm [56] for improving the system's ability to reject disturbances. On the other hand, in the present work we have employed the clock-based controller known as the *'Buehler clock'* controller [27], but we are also interested in considering other types of control schemes such as state-based controllers as well as hybrid controllers for a smooth and stable gait transition, with the aim to test new leg designs and novel controllers on the platform shown in Figure 1.

Acknowledgements

This work was partially supported by the collaborative participation in the Robotics Consortium sponsored by the U.S. Army Research Laboratory under the Collaborative Technology Alliance Program, Cooperative Agreement DAAD 19-01-2-0012. The U.S. Government is authorized to reproduce and distribute reprints for Government purposes not withstanding any copyright notation thereon.

References

[1] R. M. Alexander. *Principles of animal locomotion.* Princeton University Press, Princeton, NJ, 2003.

[2] M. H. Dickinson, C. T. Farley, R. J. Full, M. A. R. Koehl, R. Kram, and S. Lehman. How animals move: An integrative view. *Science*, 288(5463):100–106, 2000.

[3] C. T. Farley, J. Glasheen, and T. A. McMahon. Running springs: speed and animal size. *Journal of Experimental Biology*, 185:71–86, 1993.

[4] R. Blickhan and R. J. Full. Similarity in multilegged locomotion - bouncing like a monopode. *Journal of Comparative Physiology a-Sensory Neural and Behavioral Physiology*, 173(5):509–517, 1993.

[5] G. A. Cavagna, N. C. Heglund, and C. R. Taylor. Mechanical work in terrestrial locomotion: two basic mechanisms for minimizing energy-expenditure. *American Journal of Physiology-Regulatory, Integrative and Comparative Physiology*, 233(5):R243–R261, 1977.

[6] T. A. McMahon. Mechanics of locomotion. *International Journal of Robotics Research*, 3(2):4–28, 1984.

[7] R. Blickhan. The spring mass model for running and hopping. *Journal of Biomechanics*, 22(11-12):1217–1227, 1989.

[8] A. Seyfarth, H. Geyer, M. Gunther, and R. Blickhan. A movement criterion for running. *Journal of Biomechanics*, 35:649–55, 2002.

[9] R. J. Full and D. E. Koditschek. Templates and anchors: Neuromechanical hypotheses of legged locomotion on land. *Journal of Experimental Biology*, 202(23):3325–3332, 1999.

[10] R. Altendorfer, U. Saranli, H. Komsuoglu, D. Koditschek, H. B. Brown, M. Buehler, N. Moore,

D. McMordie, and R. Full. Evidence for spring loaded inverted pendulum running in a hexapod robot. In *Int. Symp. Experimental Robotics*, Honolulu, HI, USA, 2000.

[11] A. Liberman. *Running*. David & Charles Publishers, Newton Abbot, Devon, UK, 2011.

[12] R. Ringrose. Self-stabilizing running. In *Proceedings of IEEE International Conference on Robotics and Automation*, volume 1, pages 487–493, 1997.

[13] T. McGeer. Passive bipedal running. *Proceedings of the Royal Society of London Series B-Biological Sciences*, 240(1297):107–134, 1990.

[14] A. A. Biewener. *Animal locomotion*. Oxford University Press, 2003.

[15] R. Blickhan, A. Seyfarth, H. Geyer, S. Grimmer, H. Wagner, and M. Gunther. Intelligence by mechanics. *Philosophical Transactions of the Royal Society London, Series A (Mathematical, Physical and Engineering Sciences)*, 365:199–220, 2007.

[16] W. J. Schwind. *Spring loaded inverted pendulum running: A plant model*. PhD thesis, University of Michigan, Ann Arbor, MI, USA, 1998.

[17] M. Gunther, V. Keppler, A. Seyfarth, and R. Blickhan. Human leg design: optimal axial alignment under constraints. *Journal of Mathematical Biology*, 48(6):623–646, 2004.

[18] J. Rummel and A. Seyfarth. Stable running with segmented legs. *International Journal of Robotics Research*, 27:919–34, 2008.

[19] A. Seyfarth, F. Iida, R. Tausch, M. Stelzer, O. von Stryk, and A. Karguth. Towards bipedal jogging as a natural result of optimizing walking speed for passively compliant three-segmented legs. *International Journal of Robotics Research*, 28:257–65, 2009.

[20] D. P. Ferris and C. T. Farley. Interaction of leg stiffness and surface stiffness during human hopping. *Journal of Applied Physiology*, 82(1):15–22, 1997.

[21] C. T. Farley, H. H. P. Houdijk, C. Van Strien, and M. Louie. Mechanism of leg stiffness adjustment for hopping on surfaces of different stiffnesses. *Journal of Applied Physiology*, 85(3):1044–1055, 1998.

[22] D. P. Ferris, M. Louie, and C. T. Farley. Running in the real world: adjusting leg stiffness for different surfaces. *Proceedings of the Royal Society of London Series B-Biological Sciences*, 265(1400):989–994, 1998.

[23] T. A. McMahon and G. C. Cheng. The mechanics of running: how does stiffness couple with speed. *Journal of Biomechanics*, 23:65–78, 1990.

[24] A. Arampatzis, G. P. Bruggemann, and V. Metzler. The effect of speed on leg stiffness and joint kinetics in human running. *Journal of Biomechanics*, 32(12):1349–1353, 1999.

[25] C. T. Farley, R. Blickhan, J. Saito, and C. R. Taylor. Hopping frequency in humans - a test of how springs set stride frequency in bouncing gaits. *Journal of Applied Physiology*, 71(6):2127–2132, 1991.

[26] C. T. Farley and O. Gonzalez. Leg stiffness and stride frequency in human running. *Journal of Biomechanics*, 29(2):181–186, 1996.

[27] J. Y. Jun and J. E. Clark. Dynamic stability of variable stiffness running. In *Proceedings of IEEE International Conference on Robotics and Automation*, pages 1756–1761, 2009.

[28] M. Zinn, O. Khatib, B. Roth, and J. K. Salisbury. Playing it safe. *IEEE Robotics and Automation Magazine*, 11(2):12–21, 2004.

[29] B. Vanderborght, B. Verrelst, R. Van Ham, M. Van Damme, P. Beyl, and D. Lefeber. Development of a compliance controller to reduce energy consumption for bipedal robots. *Autonomous Robots*, 24:419–434, 2008.

[30] S. Riese and A. Seyfarth. Stance leg control: variation of leg parameters supports stable hopping. *Bioinspiration & Biomimetics*, 7(1):016006 (10pp), 2012.

[31] M. H. Raibert. *Legged robots that balance*. The MIT Press, 1986.

[32] M. de Lasa and M. Buehler. Dynamic compliant quadruped walking. In *Proceedings of IEEE International Conference on Robotics and Automation*, pages 3153–3158, 2001.

[33] S. Kim, J. E. Clark, and M. R. Cutkosky. isprawl: design and tuning for high-speed autonomous open-loop running. *International Journal of Robotics Research*, 25:903–912, 2006.

[34] Y. Fukuoka and H. Kimura. Dynamic locomotion of a biomorphic quadruped 'tekken' robot using various gaits: walk, trot, free-gait and bound. *Applied Bionics and Biomechanics*, 6:63–71, 2009.

[35] Z. G. Zhang and H. Kimura. Rush: a simple and autonomous quadruped running robot. *Proceedings of the Institution of Mechanical Engineers, Part I (Journal of Systems and Control Engineering)*, 223:323–36, 2009.

[36] U. Saranli, M. Buehler, and D. E. Koditschek. RHex: A simple and highly mobile hexapod robot. *International Journal of Robotics Research*, 20(7):616–631, 2001.

[37] E. Z. Moore. Leg design and stair climbing control for the rhex robotic hexapod. Master's thesis, McGill University, Montreal, Canada, 2002.

[38] J. D. Weingarten, R. E. Groff, and D. E. Koditschek. A framework for the coordination of legged robot gaits. In *Proceedings of IEEE Conference on Robotics, Automation and Mechatronics*, pages 679–686, 2004.

[39] E. Sayginer. Modelling the effects of half circular compliant legs on the kinematics and dynamics of a legged robot. Master's thesis, Middle East Technical University, Ankara, Turkey, 2010.

[40] M. M. Ankarali, E. Sayginer, Y. Yazicioglu, A. Saranli, and U. Saranli. A dynamic model of running with a half-circular compliant leg. In *Proceedings of Climbing and Walking Robots (CLAWAR)*, 2012.

[41] K.-J. Huang and P.-C. Lin. Rolling SLIP: A model for running locomotion with rolling contact. In *IEEE/ASME International Conference on Advanced Intelligent Mechatronics*, pages 21–26, 2012.

[42] B. R. Whittington and D. G. Thelen. A simple mass-spring model with roller feet can induce the ground reactions observed in human walking. *Journal of Biomechanical Engineering-Transactions of the ASME*, 131(1):011013/1–011013/8, 2009.

[43] H. Komsuoglu. Towards a comprehensive infrastructure for construction of modular and extensible robotic systems. Technical report, Dept. of Computer and Information Science, University of Pennsylvania, 2007.

[44] K. C. Galloway. *Passive variable compliance for dynamic legged robots*. PhD thesis, University of Pennsylvania, Philadelphia, PA, USA, 2010.

[45] L. L. Howell. *Compliant mechanisms*. John Wiley and Sons, Inc., 2001.

[46] K. C. Galloway, J. E. Clark, and D. E. Koditschek. Design of a multi-directional variable stiffness leg for dynamic running. In *ASME International Mechanical Engineering Congress and Exposition*, 2007.

[47] K. C. Galloway, J. E. Clark, and D. E. Koditschek. Design of a tunable stiffness composite leg for dynamic locomotion. In *Proceedings of the ASME IDETC/CIE*, 2009.

[48] J. Seipel and P. Holmes. A simple model for clock-actuated legged locomotion. *Regular & Chaotic Dynamics*, 12(5):502–520, 2007.

[49] R. Altendorfer, R. M. Ghigliazza, P. Holmes, and D. E. Koditschek. Exploiting passive stability for hierarchical control. In *5th International Conference on Climbing and Walking Robots (CLAWAR)*, 2002.

[50] Y. Aydin, K. C. Galloway, Y. Yazicioglu, and D. E. Koditschek. Modeling the compliance of a variable stiffness C-shaped leg using Castigliano's theorem. In *Proceedings of the ASME IDETC/CIE*, Montreal, Quebec, Canada, 2010.

[51] L. L. Howell and A. Midha. Parametric deflection approximations for initially curved, large-deflection beams in compliant mechanisms. In *Proceedings of the ASME DETC*, Irvine, California, 1996.

[52] J. D. Weingarten, G. A. D. Lopes, M. Buehler, R. E. Groff, and D. E. Koditschek. Automated gait adaptation for legged robots. In *Proceedings of IEEE International Conference on Robotics and Automation*, 2004.

[53] J. Guckenheimer and P. Holmes. *Nonlinear oscillations, dynamical systems, and bifurcations of vector fields*, volume 42 of *Applied Mathematical Sciences*. Springer-Verlag, New York, 1983.

[54] J. A. Nelder and R. Mead. A simplex-method for function minimization. *Computer Journal*, 7(4):308–313, 1965.

[55] G. Gabrielli and T. von Karman. What price speed. *Mechanical Engineering*, 72(10):775–781, 1950.

[56] D. G. E. Hobbelen and M. Wisse. A disturbance rejection measure for limit cycle walkers: The gait sensitivity norm. *IEEE Transactions on Robotics*, 23(6):1213–1224, 2007.